applied sciences

MDPI

Article

Experimental Study on Maximum Dynamic Shear Modulus of Yangtze River Overconsolidated Floodplain Soft Soils

Yifeng Zhou, Xing Xiao, Zhenglong Zhou and Qi Wu *

Institute of Geotechnical Engineering, Nanjing Tech University, Nanjing 211899, China
* Correspondence: qw09061801@163.com

Abstract: This study conducted experimental tests on the undisturbed Nanjing Yangtze River floodplain soft soil using the bender element instrument to determine the maximum dynamic shear modulus of the Yangtze River floodplain overconsolidated soft soil. The $G_{\max}$ of floodplain soft soil with different overconsolidated ratio OCR, initial effective confining pressure σ_{3c}', and void ratio e are discussed. The results indicated that $G_{\max}$ reduced as e rose for given σ_{3c}' and OCR. In addition, an increase in OCR contributed to a gradual decrease in the decay rate of $G_{\max}$, while the $G_{\max}$ decay rate is insensitive to the change of σ_{3c}'. The void ratio-normalized maximum shear modulus $G_{\max}/F(e)$ improved with the increase in the stress-normalized initial effective confining pressure σ_{3c}'/P_a, whereas the growth rate gradually drops, and a power relationship is then obtained between $G_{\max}/F(e)$ and σ_{3c}'/P_a. Based on the regression analysis, a $G_{\max}$ prediction method is established for reasonably characterizing Yangtze River floodplain soft soils with various over-consolidation states, initial stress conditions, and compactness levels, with a prediction error of less than 10%.

Keywords: floodplain soft soil; overconsolidated ratio; Initial effective confining pressure; void ratio; bender element testing

check for updates

Citation: Zhou, Y.; Xiao, X.; Zhou, Z.; Wu, Q. Experimental Study on Maximum Dynamic Shear Modulus of Yangtze River Overconsolidated Floodplain Soft Soils. *Appl. Sci.* **2023**, *13*, 4733. https://doi.org/10.3390/app13084733

Academic Editors: Sang-Hyo Kim, Xianwei Zhang, Xinyu Liu and Ran An

Received: 10 March 2023
Revised: 30 March 2023
Accepted: 6 April 2023
Published: 9 April 2023

1. Introduction

Floodplain soils formed by unstable sedimentary environments are widespread in rivers, lakes, coasts, and other landforms. Foundations of bridges, offshore projects, and sub-sea tunnels will inevitably pass through this type of soil. However, under the reciprocal influence of the water flow or wave, the floodplain soils exhibit distinctive horizontal stratification and depositional rhythm. They are characterized by a high water content, large porosity ratio, high compressibility, and an evident over-consolidation state. The floodplain soils are susceptible to residual deformation or strength damage caused by waves and earthquakes, essential to soil subsidence and building instability. $G_{\max}$ (defined as the dynamic shear modulus G when the shear strain level is less than 10^{-5}, with the soil deformation belonging to the elastic range) is a fundamental parameter for describing the dynamic properties of soils, and it plays a vital role in geotechnical problems such as soil deformation prediction, potential liquefaction evaluation, seismic site response analysis, and dynamic foundation design parameters [1–4]. Therefore, conducting a systematic study on the $G_{\max}$ of overconsolidated floodplain soft soils is necessary.

Extensive studies have been conducted to investigate the $G_{\max}$ of soils using resonant column (RC) and bender element (BE) tests [5–7]. The level of densification (void ratio e or relative density D_r) and the initial effective confining pressure σ_{3c}' is surely the most fundamental effects on $G_{\max}$ [8–10]. However, the effect of frequency f on $G_{\max}$ is controversial. Kim and Stokoe [11] proposed that an increase in f will lead to an increase in G of clayey soils in the range 0.001 Hz < f < 200 Hz, while Irfan [12] insisted that the f range of 10~100 Hz did not have a significant effect on G. In this paper, the effect of e and σ_{3c}' was considered instead of f. For sandy soils, Hardin and Black [13] indicated, based on a large number of RC tests, that $G_{\max}$ rises as σ_{3c}' increases and decreases as e improves.

Kim and Novak [14] confirmed the effect of σ_{3c}', e, and other factors on G_{max}. Payan and Chenari [15] and Liu et al. [16] demonstrated that stress anisotropy and the particle shape of soils can still affect G_{max}.

Gu et al. [17] conducted a series of combined cyclic triaxial and bender element tests regarding clayey soils. They revealed that cyclic stress and strain history lead to a decrease in G_{max}, while the reduction in G_{max} in the strain-controlled tests is less than that in the stress-controlled tests. Kokusho and Yoshida [18] reported that factors such as stress history (OCR) and plasticity index (I_p) also have some influence on the G_{max}. Vucetic and Dobry [19] exhibited that G_{max} does not change with I_p for normally consolidated clays (OCR = 1), and for overconsolidated clays (OCR > 1), G_{max} increases with I_p. Marika et al. [20] also explored the effect of the initial consolidation path on the G_{max} of Boston blue clay. Laureano et al. [21] examined the impact of moisture content (w) and consolidation time (T) on the G_{max} of Texas-expanded clay and established an empirical equation considering these two factors. Lin et al. [22] investigated the influence of montmorillonite to kaolinite (M-K) ratio and T on the G_{max} of clay soils. Sadeghzadegan et al. [23] discovered that the G_{max} initially decreases as clay content increases from 0 to 20% and then rises slightly as clay content ranges from 20 to 30%. In addition, under the same clay content, the G_{max} enhances when the degree of saturation drops from 100 to 95%. Kantesaria and Sachan [24] indicated that the G_{max} of compacted high-plasticity clay is related to the mean effective stress and slightly depends on deviatoric stress. Simultaneously, G_{max} decreases as the strain level increases during shearing. The above studies provide valuable research values and scientific insights for investigating soft soil's dynamic properties.

As regional soft soils, research on the dynamic properties of the Yangtze River floodplain soft soil is still limited, particularly because the knowledge of shear modulus remains inadequate. G_{max} is the most fundamental parameter for describing the dynamic soil properties, essential for analyzing the seismic response and soil-structure dynamic interaction. This study conducts a series of BE tests to investigate the G_{max} of overconsolidated soft soils in the Yangtze River floodplain. A G_{max} prediction method is developed for reasonably characterizing Yangtze River floodplain soft soils with various over-consolidation states, initial stress conditions, and compactness levels. This study can provide primary data for the engineering and construction requirements of the Yangtze River floodplain.

2. Maximum Dynamic Shear Modulus Tests

2.1. Tested Materials

Floodplain soft soil is extensively dispersed clay formed in the late Quaternary period that is commonly characterized by high moisture content, high void ratio, and low permeability due to many factors, including environment, stress history, and structural properties and can be quaking when the vibration level is high. As depicted in Figure 1, the samples tested in this study belong to typical Yangtze River floodplain soft soils, which are gray-brown and have an apparent horizontal layer texture and sand trap structure. The original soil is air-dried, milled, and sieved, resulting in the formation of loose particles. The soft soils in the diffuse phase are composed entirely of clay with grain sizes less than 0.075 mm, except for the sand layer, which is fine sand.

Figure 1. Undisturbed Yangtze River floodplain facies soft soil.

Figure 2 illustrates the SEM image of the soft soil in the Yangtze River floodplain. It indicates that the original soft soil is mostly agglomerate or flaky aggregates microscopically. Its surface is frequently covered with a loose arrangement of clay particles in the form of stacked flakes. In addition to agglomerates and clumps of mucilage, several highly angular and irregular powder particles are visible. In the relationship between the structure and these agglomerates or granular aggregates, direct contact linkage, bonding material linkage, edge-surface, and point-surface contact play the most critical roles.

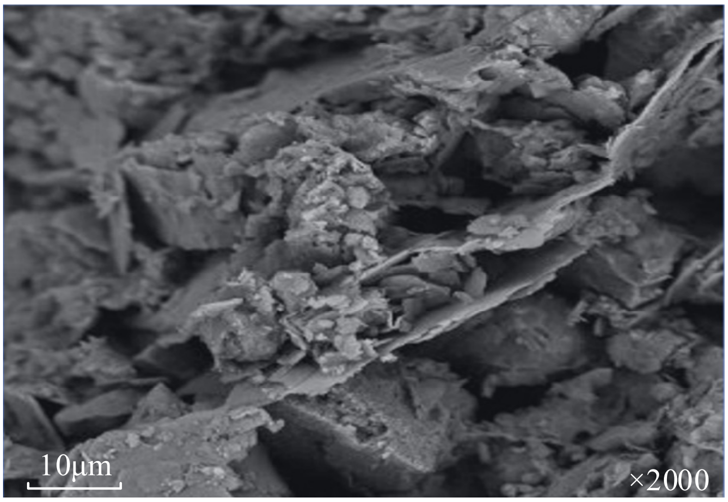

Figure 2. Microstructure of undisturbed Yangtze River floodplain facies soft soil.

Long-term hydraulic transport dominates the sedimentation of Yangtze River floodplain soft soil, which has high dispersibility, hydrophilicity, moisture content, void ratio, compressibility, sensitivity, and generally creeping and thixotropic properties. The physical analysis also demonstrated that the clay minerals species are single, mainly with illite (70%) and chlorite (21.8%), and the clastic minerals are mainly quartz (5.5%) and feldspar (2.7%), and the material composition is unified.

2.2. Specimen Preparation, Saturation, and Consolidation

The Yangtze River floodplain's soft soil is mainly distributed between 5 and 25 m below the surface. The typical original floodplain soft soils, 51 in total, were extracted using an open-end thin-wall sampler. Because the underground water level is about 1–2 m, all the undisturbed samples are saturated soils. Table 1 lists the fundamental physical and mechanical properties of the soft soils in each drill hole. The density ρ, moisture content w, void ratio e, and plasticity index I_p are measured using ASTM D4318 [25]. It indicates that the w values of the floodplain soft soils are between 37 and 42%, and I_p is distributed between 14.8 and 17.8. The samples are classified into four groups based on the depth H of the samples: Group A: H = 5–10 m; Group B: H = 10–15 m; Group C: H = 15–20 m; Group D: H = 20–25 m. σ_{3c}' was set to 50, 85, 120, and 150 kPa for samples in groups A, B, C, and D, respectively. The consolidation of each group was performed with OCR = 1, 2, and 3 in combination with the e distribution in each group. Table 1 details the test conditions.

Table 1. Basic physical properties of test soil samples.

No.	H (m bgs)	ρ (g·cm^{-3})	w (%)	e (-)	LL (%)	PL (%)	I_p (%)	Grain size Sand [a] (%)	Silt [b] (%)	Clay [c] (%)	$\sigma_{3c}{}'$ (kPa)	OCR (-)
A1	8.7–8.9	1.39	39.32	0.95	38.1	21.8	16.3	25.8	59.8	14.4	50	1
A2	6.8–7.0	1.27	40.11	1.10	49.7	32.5	17.2	16.6	64	19.4	50	1
A3	6.3–6.5	1.31	41.08	1.04	37.8	20.4	17.4	12.6	63.7	23.7	50	1
A4	8.3–8.5	1.27	40.14	1.13	35.4	18.5	16.9	12.5	70.3	17.2	50	1
A5	8.2–8.4	1.33	38.81	1.03	34.4	17.6	16.8	12.5	66.9	20.6	50	2
A6	7.7–7.9	1.29	42.61	1.08	36.9	20.1	16.8	19.9	59	21.1	50	2
A7	9.2–9.4	1.26	41.43	1.12	39.4	22.0	17.4	46.8	39.3	13.9	50	2
A8	7.4–7.7	1.26	40.43	1.15	37.1	20.1	17.0	19.9	59	21.1	50	2
A9	7.3–7.5	1.30	39.55	1.09	37.6	20.1	17.5	19.9	59	21.1	50	3
A10	8.3–8.5	1.33	40.84	1.03	39.0	21.8	17.2	25.8	59.8	14.4	50	3
A11	7.8–8.0	1.26	41.45	1.13	36.3	19.0	17.3	13.8	55	31.2	50	3
A12	5.4–5.6	1.39	42.94	0.96	38.1	21.3	16.8	9.0	66.3	24.7	50	3
B1	13.7–13.9	1.36	40.06	0.97	42.1	24.7	17.4	8.9	68.7	22.4	85	1
B2	14.5–14.7	1.33	39.91	1.04	38.2	21.9	16.3	5.4	74.5	20.1	85	1
B3	14.5–14.7	1.29	40.5	1.09	39.5	21.9	17.6	5.4	74.5	20.1	85	1
B4	12.5–12.7	1.25	40.26	1.14	35.2	18.7	16.5	31.8	51.2	17.0	85	1
B5	14.1–14.3	1.26	39.59	1.16	39.0	22.1	16.9	6.8	76.3	16.9	85	1
B6	14.3–14.5	1.34	40.42	1.01	36.9	20.4	16.5	10.0	64.7	25.3	85	2
B7	13.1–13.3	1.3	40.14	1.08	34.7	18.0	16.7	15.9	66.3	17.8	85	2
B8	14.8–15.0	1.31	41.05	1.09	31.5	14.5	17.0	2.1	76.4	21.5	85	2
B9	14.7–14.9	1.25	41.27	1.14	39.1	21.9	17.2	5.4	74.5	20.1	85	2
B10	13.8–14.0	1.19	40.6	1.26	41.4	24.7	16.7	8.9	68.7	22.4	85	2
B11	14.5–14.7	1.35	38.87	1.02	42.7	27.6	15.1	1.1	77.8	21.1	85	3
B12	13.1–13.3	1.30	38.43	1.09	35.2	18.0	17.2	15.9	66.3	17.8	85	3
B13	13.5–13.7	1.27	40.21	1.12	41.4	24.7	16.7	8.9	68.7	22.4	85	3
B14	14.9–15.1	1.24	41.7	1.14	40.5	23.6	16.9	7.4	76.8	15.8	85	3
C1	15.4–15.6	1.40	42.41	0.95	38.9	21.8	17.1	30.6	48.5	20.9	120	1
C2	17.1–17.3	1.31	38.42	1.04	39.5	23.3	16.2	5.6	67.3	27.1	120	1
C3	16.1–16.3	1.29	41.38	1.08	39.3	23.0	16.3	7.9	66.3	25.8	120	1
C4	15.3–15.5	1.27	39.33	1.13	41.4	23.6	17.8	7.4	76.8	15.8	120	1
C5	16.2–16.4	1.27	38.31	1.15	39.3	23.0	16.3	7.9	66.3	25.8	120	1
C6	15.7–15.9	1.32	39.87	1.03	39.9	23.0	16.9	7.9	66.3	25.8	120	2
C7	15.1–15.3	1.29	40.24	1.08	39.0	21.9	17.1	4.9	69.3	25.8	120	2
C8	15.8–16.0	1.28	36.93	1.11	38.4	23.0	15.4	7.9	66.3	25.8	120	2
C9	16.5–16.7	1.25	41.66	1.13	34.0	16.8	17.2	11.1	24.4	64.5	120	2
C10	16.3–16.5	1.32	37.17	1.03	32.7	16.8	15.9	11.1	24.4	64.5	120	3
C11	15.2–15.4	1.3	39.24	1.08	38.4	23.6	14.8	7.4	76.8	15.8	120	3
C12	15.6–15.8	1.28	40.92	1.12	40.5	23.0	17.5	7.9	66.3	25.8	120	3
C13	15.7–15.9	1.26	39.82	1.14	39.4	23.0	16.4	7.9	66.3	25.8	120	3
D1	21.1–21.3	1.35	41.43	0.99	37.7	20.2	17.5	3.4	72.2	24.4	150	1
D2	22.3–22.5	1.33	40.92	1.05	37.7	21.2	16.5	3.2	72.2	24.6	150	1
D3	23.1–23.3	1.28	41.59	1.11	40.9	23.8	17.1	3.4	74.9	21.7	150	1
D4	23.8–24.0	1.26	40.92	1.15	41.2	23.7	17.5	3.4	73.2	23.4	150	1
D5	21.6–21.8	1.23	41.66	1.18	39.3	22.3	17.0	3.4	83.4	13.2	150	2
D6	22.5–22.7	1.27	39.45	1.11	39.6	22.5	17.1	5.0	69.5	25.5	150	2
D7	23.3–23.5	1.3	41.11	1.05	39.1	21.8	17.3	4.4	83.4	12.2	150	2
D8	23.8–24.0	1.38	38.23	0.98	37.9	21.5	16.4	8.6	68.2	23.2	150	2
D9	21.9–22.1	1.37	39.83	0.95	40.4	23.8	16.6	3.4	85.2	11.4	150	3
D10	22.9–23.1	1.33	40.14	1.03	38.1	20.3	17.8	15.6	60.9	23.5	150	3
D11	23.4–23.6	1.28	39.82	1.1	37.5	20.4	17.1	14.5	71.7	13.8	150	3
D12	24.6–24.8	1.25	38.92	1.16	38.3	20.9	17.4	3.4	83.4	13.2	150	3

Note: 'bgs' means 'below ground surface,' LL = liquid limit, PL = plastic limit. [a] The grain size of sand particles ranges from 0.075~0.1 mm. [b] The grain size of silt particles ranges from 0.005~0.075 mm. [c] The grain size of clay particles is below 0.005 mm.

The standard dimensions of samples (50 × 100 mm) were prepared and saturated using the vacuum saturation method according to the ASTM D5311-13 [26]. The samples were saturated in the saturation vessel for 10 h. Then, the specimen was placed in the apparatus, and the back pressure saturation was conducted. Back pressure was applied step by step until the value of Skempton's B was greater than 0.97, which can guarantee the saturation to prevent differences in sample preparation from affecting the test results. Then they were placed in the pressure chamber and consolidated according to the corresponding consolidation conditions. When the average strain rate of the soil sample was less than

$1 \times 10^{-3}\%/\text{min}$, consolidation was achieved, followed by the bender element test. The time of consolidation was about 4~5 days.

2.3. Testing Apparatus and Process

The bender element measurement system installed in the GCTS HCA-300 static and dynamic triaxial instrument is used for the test. The bender element includes two piezoelectric ceramic sheets and a central copper stiffening layer. During the test, two bender elements, excitation and receiving, are installed at both ends of the soil sample. The excitation element produces horizontal vibration under the excitation of a specific pulse voltage. In addition, the shear wave reaches the receiving element following the sample propagation. A weak electrical signal is generated at this time, and the oscilloscope can calculate the propagation time (t) of the shear wave. A series of sinusoid signals from 1 to 40 kHz was used as the excitation, and the received signals corresponding to these excitation frequencies were examined to better identify the t. The 10 kHz excitation signal consistently yielded a clear arrival of the shear wave for floodplain soft soils. This is in good agreement with the observation of Yang and Liu [27] and Chen et al. [28]. The height of the soil sample minus the length of the bender element deep into the soil body can be utilized to calculate the shear wave propagation distance and thus determine the shear wave velocity. The equation for calculating the soil shear wave velocity (Vs) using the indoor bender element test is:

$$V_s = L_0/t \tag{1}$$

where $L_0 = L - L_b$, L is the height of the sample; L_b is the length of the bender element deep into the soil; t is the propagation time.

Calculating the shear wave velocity (V_s) and the maximum dynamic shear modulus G_0 requires accurately determining the shear wave's arrival time. Different scholars have proposed various analytical methods for identifying the shear wave arrival time. The widely used methods are the time-domain initial wave, peak-to-peak, and intercorrelation methods. Brigonoli et al. [29], Lee et al. [30], and Zhou et al. [31] indicated that the shear wave velocity propagation time t could be determined easily and accurately using the time-domain initial wave method. In this experiment, a sinusoidal pulse frequency of 10 kHz was applied, and the shear wave always arrived clearly and effectively under the excitation frequency of 10 kHz. The time domain initial wave approach is employed to determine the arrival time of shear wave velocity, i.e., depending on the first turning point A of the received signal as the arrival point of the shear wave. Figure 3 depicts a typical bender element test received signal diagram. After determining $V_{s.}$ for each sample, the following equation is utilized to calculate G_{max} according to elastic theory:

$$G_{max} = \rho V_s^2 \tag{2}$$

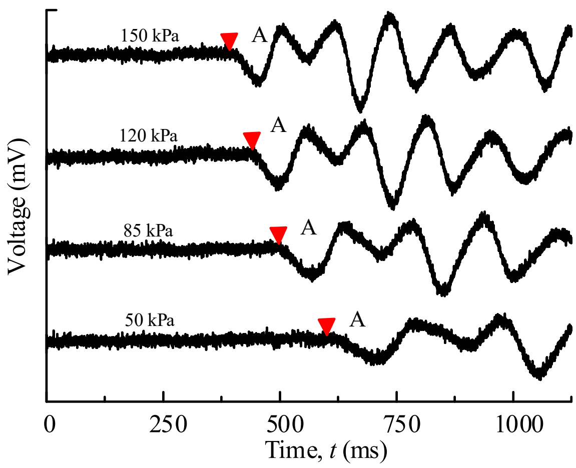

Figure 3. Typical time histories of output signals from bender element tests.

3. Test Results and Analysis

Figure 4 illustrates the relationship between the G_{max} and e for the Yangtze River floodplain's soft soils under different $\sigma_{3c}{}'$. For the given $\sigma_{3c}{}'$ and OCR, G_{max} decreases as e increases. This is because the smaller e is, the looser the soil, the weaker the cohesion and cementation between the particles, the more open the pores in the soil, and the more unstable the soil structure, leading to the smaller G_{max}. In addition, under the same $\sigma_{3c}{}'$ and e, G_{max} improves with increasing OCR, revealing that the G_{max} is larger, the higher the pre-consolidation pressure. When Figure 4a–d are combined with the given e and OCR, G_{max} rises as $\sigma_{3c}{}'$ grows. The increase in $\sigma_{3c}{}'$ has a noticeable hoop-tightening effect on the soil, which can reduce the void ratio of the soil and strengthen the bond between soil particles. The greater the effective envelope pressure, the greater the soil sample's resistance to shear deformation, as measured by an increase in G_{max}. In each graph, three red trend lines represent the effect of e on G_{max}, respectively, and Jamiolkowski et al. [32] proposed the equation $F(e)$ to characterize the effect of e on G_{max}.

$$F(e) = e^{-d} \tag{3}$$

where d is the fitting parameter characterizing the effect of increasing e on the degree of G_{max} decay. When $\sigma_{3c}{}'$ and OCR are constants, d can be determined using regression analysis, and the corresponding values of d are displayed in Figure 5. It reveals that under the same OCR, the increase in $\sigma_{3c}{}'$ does not significantly affect d, which remains nearly constant. As OCR rises, d reduces gradually, with d values of 2.981, 2.523, and 2.055 for OCR = 1, 2, and 3, respectively. This indicates that the decay rate of G_{max} with e is independent of $\sigma_{3c}{}'$ but decreases as OCR grows.

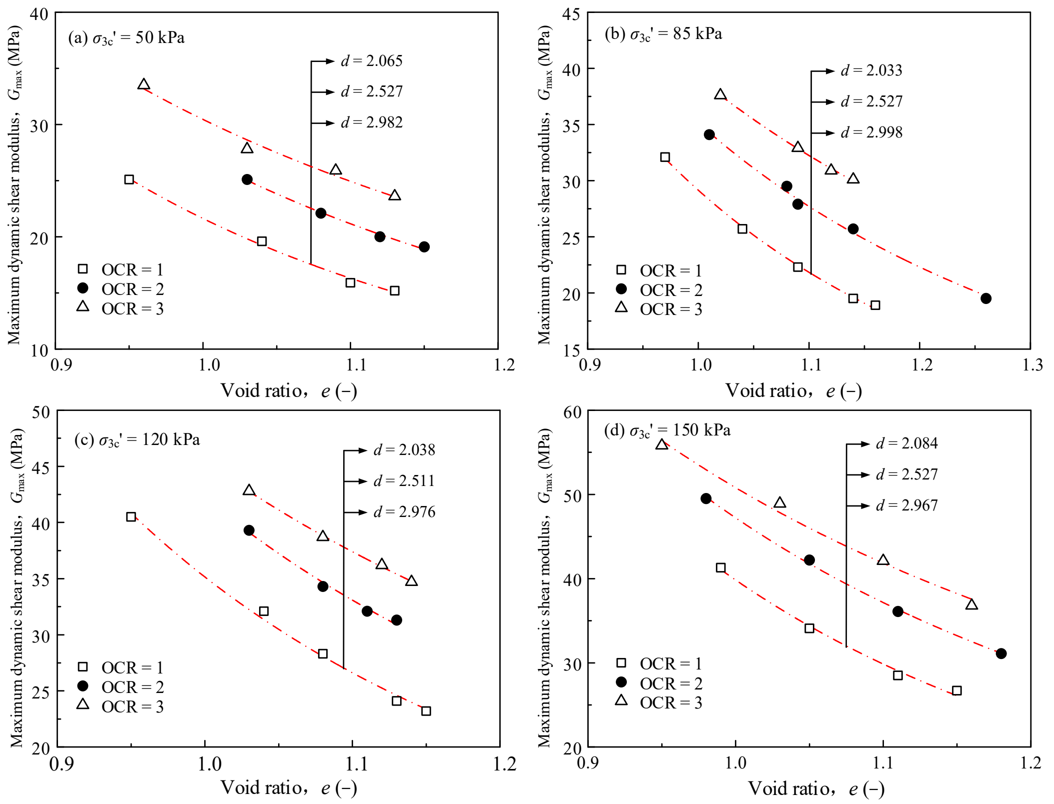

Figure 4. The relationship between G_{max} and e under different $\sigma_{3c}{}'$: (**a**) $\sigma_{3c}{}'$ = 50 kPa, (**b**) $\sigma_{3c}{}'$ = 85 kPa,. (**c**) $\sigma_{3c}{}'$ = 120 kPa, (**d**) $\sigma_{3c}{}'$ = 150 kPa.

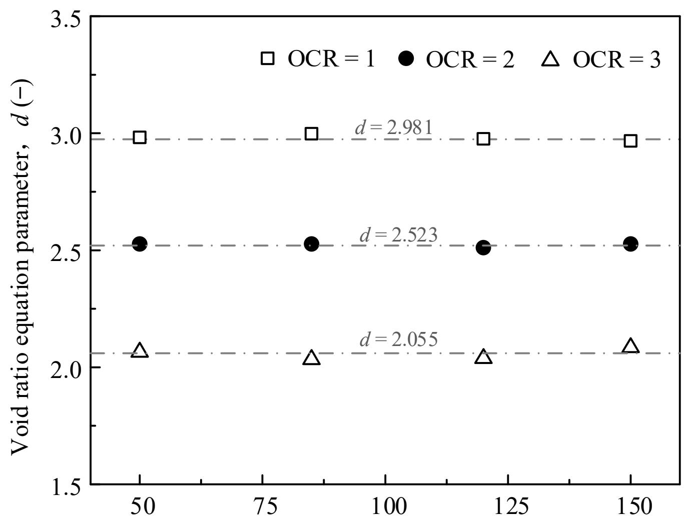

Figure 5. Relationship between d and $\sigma_{3c}{}'$ with different OCR.

Figure 6 displays the relationship between the normalized maximum shear modulus $G_{max}/F(e)$ and the normalized initial effective confining pressure $\sigma_{3c}{}'/P_a$, where P_a is the standard atmospheric pressure, assumed to be 100 kPa. For given OCR, $G_{max}/F(e)$ grows as $\sigma 3c'/Pa$ improves, but the growth rate gradually decreases, and a power function can describe the relationship between $G_{max}/F(e)$ and $\sigma_{3c}{}'/P_a$:

$$G_{max} = AF(e)(\sigma_{3c}{}'/P_a)^n \tag{4}$$

where A is a measured fitting parameter whose value corresponds to the $G_{max}/F(e)$ value of the floodplain's soft soil at $\sigma 3c'$ = 100 kPa; n is the stress index, describing the influence of $\sigma_{3c}{}'$ on $G_{max}/F(e)$. In addition, the $G_{max}/F(e) \sim \sigma_{3c}{}'/P_a$ relationship curve gradually shift upward as the OCR increases, with the A value gradually increasing from 31.8 to 42.0 MPa and n decreasing from 0.552 to 0.465 as the OCR rises from 1 to 3.

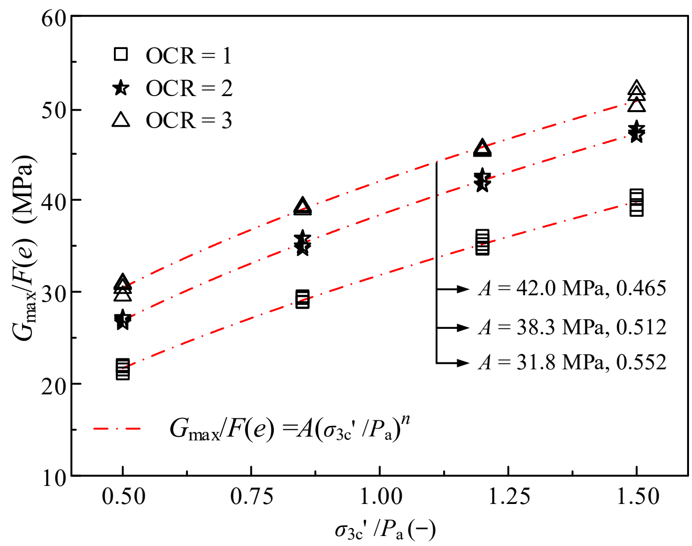

Figure 6. Relationship between $G_{max}/F(e)$ and $\sigma_{3c}{}'/P_a$.

Figures 5 and 6 demonstrate that the OCR significantly impacts the fitted parameters d, A, and n. In contrast, Figure 7 shows that as OCR enhances, d grows linearly, A rises, and n decreases linearly. The following equations give the relationship between d, A, n, and OCR:

$$d = 0.463 \times \text{OCR} + 1.594 \tag{5}$$

$$A = 31.9 \times \text{OCR}^{0.255} \tag{6}$$

$$n = -0.043 \times \text{OCR} + 0.597 \tag{7}$$

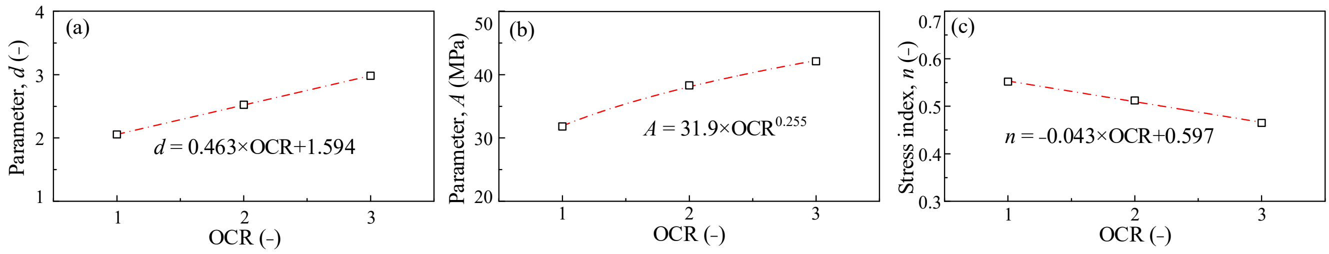

Figure 7. The relationship between parameters d, A, n, and OCR: (**a**) d versus OCR, (**b**) A versus OCR, (**c**) n versus OCR.

The $G_{\max}$ prediction equation that integrates and considers OCR, e, and $\sigma_{3c}{}'$ can be established by combining Equations (3) and (4).

$$G_{\max} = 31.9\text{OCR}^{0.255} \times e^{-0.463\text{OCR}+1.594} \times (\sigma_{3c}{}'/P_{a})^{-0.043\text{OCR}+0.597} \tag{8}$$

Based on this prediction equation, the values of $G_{\max}$ of the Yangtze River overconsolidated floodplain's soft soils are predicted by the following step:

Step 1: Determining the effective stress, $\sigma_{3c}{}'$, based on the depth of the soil extracted in situ.

Step 2: Identifying the void ratio, e, from laboratory experiments.

Step 3: Calculating the value of the per-consolidation pressure on the compression curve ($e - p$ curve) using the Casagrande method and computing the over-consolidation ratio, OCR.

Step 4: Based on the modified $\sigma_{3c}{}'$, e, OCR, estimating $G_{\max}$ using Equation (8).

Figure 8 compares the $G_{\max}$ tested and predicted values from Equation (8). For Yangtze River floodplain soft soils with various e, $\sigma_{3c}{}'$, and OCR, the difference of $G_{\max}$ predicted values using the proposed evaluation model is less than 10%. Liang et al. [33] developed a $G_{\max}$ prediction model for sand with different values of relative densities, D_r, and the deviation between the predicted and the measured values of $G_{\max}$ was within a range of 20%. Zhang et al. [34] established a $G_{\max}$ prediction model for marine soils, and the deviation between predicted and measured values of $G_{\max}$ was within a range of 15%. Therefore, it is encouraging that the theoretically estimated $G_{\max}$ of Yangtze River floodplain soft soils (Equation (8)) coincide well with the experimentally measured $G_{\max}$ values. The significant implication of this study is that the predicted Gmax of Yangtze River floodplain soft soils serve as a valuable reference for the site seismic response analysis in the Yangtze delta region.

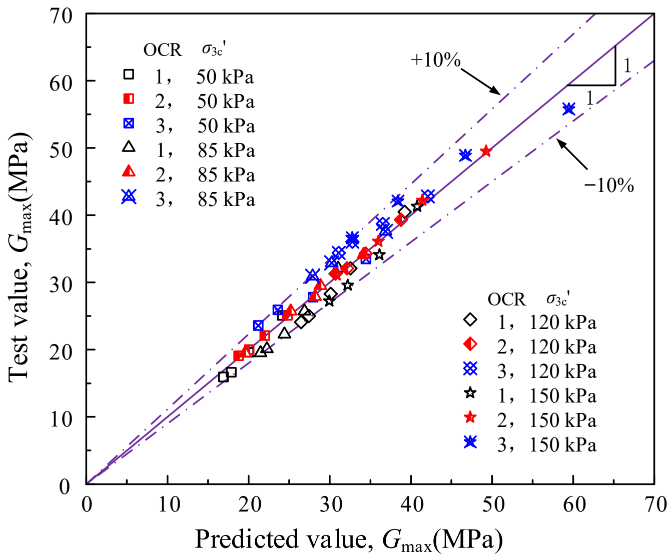

Figure 8. Comparison of G_{max} predicted values and test values.

4. Conclusions

The maximum dynamic shear modulus G_{max} of Yangtze River floodplain soft soil with sand trap structure and horizontal layer texture is examined using a series of bender element tests. The effects of void ratio e, initial effective confining pressure σ_{3c}', and overconsolidated ratio OCR on G_{max} are investigated, and the analysis indicated that G_{max} decreases with e, increasing OCR causes a gradual decrease in the decay rate of G_{max} with e, whereas increasing σ_{3c}' does not affect G_{max} decay rate. Furthermore, the normalized maximum shear modulus $G_{max}/F(e)$ increases as normalized initial effective confining pressure σ_{3c}'/Pa increases. However, its growth rate gradually reduces, and $G_{max}/F(e)$ has a power function relationship with σ_{3c}'/Pa. As the OCR rises, fitting parameters d and A grow while stress index n decreases. d and n exhibit a linear correlation with OCR, whereas A has a power function relationship with OCR. Based on the regression analysis, a G_{max} prediction method is proposed to adequately characterize the Yangtze River floodplain soft soils with various over-consolidation states, initial stress conditions, and densities, with a prediction error of less than 10%.

In the future, the dynamic behavior of soft floodplain soils subjected to cyclic loading will be conducted to investigate the cyclic degradation and establish the cyclic degradation model based on G_{max}. Additionally, microcosmic tests will be performed on floodplain soft soils to explain the dynamic characteristics.

Author Contributions: Methodology, Y.Z., Z.Z. and Q.W.; Validation, X.X.; Investigation, X.X.; Writing—original draft, Y.Z.; Writing—review & editing, Z.Z. and Q.W.; Project administration, Q.W.; Funding acquisition, Q.W. All authors have read and agreed to the published version of the manuscript.

Funding: This research received no external funding.

Institutional Review Board Statement: Not applicable.

Informed Consent Statement: Not applicable.

Data Availability Statement: Data is available on request through the author named Qi Wu.

Conflicts of Interest: The authors declare that there is no conflict of interest regarding the publication of this paper.

References

1. Senetakis, K.; He, H. Dynamic characterization of a biogenic sand with a resonant column of fixed-partly fixed boundary conditions. *Soil Dyn. Earthq. Eng.* **2017**, *95*, 180–187. [CrossRef]
2. An, R.; Kong, L.; Zhang, X.; Li, C. Effects of dry-wet cycles on three-dimensional pore structure and permeability characteristics of granite residual soil using X-ray micro computed tomography. *J. Rock Mech. Geotech. Eng.* **2022**, *14*, 851–860. [CrossRef]
3. Chen, G.X.; Liang, K.; Zhao, K.; Yang, J. Shear modulus and damping ratio of saturated coral sand under generalised cyclic loadings. *Géotechnique* **2022**, 1–18. [CrossRef]
4. Wu, Q.; Wang, Z.; Qin, Y.; Yang, W. Intelligent Model for Dynamic Shear Modulus and Damping Ratio of Undisturbed Marine Clay Based on Back-Propagation Neural Network. *J. Mar. Sci. Eng.* **2023**, *11*, 249. [CrossRef]
5. He, H.; Li, M.N.; Senetakis, K. A note on influence of stress anisotropy on the Poisson's ratio of dry sand. *J. Rock Mech. Geotech. Eng.* **2017**, *9*, 1159–1164. [CrossRef]
6. Morsy, A.M.; Salem, M.A.; Elmamlouk, H.H. Evaluation of dynamic properties of calcareous sands in Egypt at small and medium shear strain ranges. *Soil Dyn. Earthq. Eng.* **2019**, *116*, 692–708. [CrossRef]
7. Subramanian, S.; Khan, Q.; Ku, T. Effect of sand on the stiffness characteristics of cement-stabilized clay. *Constr. Build. Mater.* **2020**, *264*, 120192. [CrossRef]
8. Jafarian, Y.; Javdanian, H.; Haddad, A. Dynamic properties of calcareous and siliceous sands under isotropic and anisotropic stress conditions. *Soils Found.* **2018**, *58*, 172–184. [CrossRef]
9. Yang, S.L.; Ren, Y.B.; Andersen, K.N. Effects of thixotropy and reconsolidation on the undrained shear characteristics of remoulded marine clays. *Ocean Eng.* **2021**, *239*, 109888. [CrossRef]
10. Wu, Q.; Liu, Q.F.; Zhuang, H.Y.; Xu, C.X.; Chen, G.X. Experimental investigation of dynamic shear modulus of saturated marine coral sand. *Ocean Eng.* **2022**, *264*, 112428.
11. Kim, D.S.; Stokoe, K.H. Deformational characteristics of soils at small to medium strains. In Proceedings of the First International Conference on Earthquake Geotechnical Engineering, Tokyo, Japan, 14–16 November 1995; pp. 89–94.
12. Irfan, M.; Cascante, G.; Basu, D.; LeBoeuf, D. Low-strain dynamic characterization of undisturbed Leda clay. *Can. Geotech. J.* **2022**, *59*, 631–643. [CrossRef]
13. Hardin, B.O.; Black, W.L. Vibration modulus of normally consolidated clay. *J. Soil Mech. Found. Div.* **1968**, *92*, 27–42. [CrossRef]
14. Kim, T.C.; Novak, M. Dynamic properties of some cohesive soils of Ontario. *Can. Geotech. J.* **1981**, *18*, 371–389. [CrossRef]
15. Payan, M.; Chenari, R.J. Small strain shear modulus of anisotropically loaded sands. *Soil Dyn. Earthq. Eng.* **2019**, *125*, 105726. [CrossRef]
16. Liu, J.; Otsubo, M.; Kawaguchi, Y.; Kuwano, R. Anisotropy in small-strain shear modulus of granular materials: Effects of particle properties and experimental conditions. *Soils Found.* **2022**, *62*, 101105. [CrossRef]
17. Gu, C.; Wang, J.; Cai, Y.; Guo, L. Influence of cyclic loading history on small strain shear modulus of saturated clays. *Soil Dyn. Earthq. Eng.* **2014**, *66*, 1–12. [CrossRef]
18. Kokusho, T.; Yoshida, Y.; Esashi, Y. Dynamic Properties of Soft Clay for Wide Strain Range. *Soils Found.* **1982**, *22*, 1–18. [CrossRef]
19. Vucetic, M.; Dobry, R. Effect of soil plasticity on cyclic response. *J. Geotech. Geoenviron. Eng.* **1991**, *117*, 89–107. [CrossRef]
20. Santagata, M.; Germaine, J.T.; Ladd, C.C. Factors affecting the initial stiffness of cohesive soils. *J. Geotech. Geoenviron. Eng.* **2005**, *131*, 430–441. [CrossRef]
21. Hoyos, L.R.; Puppala, A.J.; Chainuwat, P. Dynamic Properties of Chemically Stabilized Sulfate Rich Clay. *J. Geotech. Geoenviron. Eng.* **2004**, *130*, 153–162. [CrossRef]
22. Lin, P.; Ni, J.-J.; Garg, A.; Yu, S.-M. Effects of Clay Minerals on Small-Strain Shear Modulus and Damping Ratio of Saturated Clay. *Soil Mech. Found. Eng.* **2020**, *57*, 105–109. [CrossRef]
23. Sadeghzadegan, R.; Naeini, S.A.; Mirzaii, A. Effect of clay content on the small and mid to large strain shear modulus of an unsaturated sand. *Eur. J. Environ. Civ. Eng.* **2020**, *24*, 631–649. [CrossRef]
24. Kantesaria, N.; Sachan, A. Small-strain shear modulus and yielding characteristics of compacted high-plasticity clay. *Géotechnique* **2022**, *72*, 424–437. [CrossRef]
25. *D4318-17E01*; Standard test method for sand content by volume of bentonitic slurries. ASTM International: West Conshohocken, PA, USA, 2017.
26. *D5311-13*; Standard Test Method for Load Controlled Cyclic Triaxial Strength of Soil. ASTM International: West Conshohocken, PA, USA, 2013.
27. Yang, J.; Liu, X. Shear wave velocity and stiffness of sand: The role of non-plastic fines. *Géotechnique* **2016**, *66*, 500–514. [CrossRef]
28. Chen, G.X.; Wu, Q.; Zhao, K.; Shen, Z.F.; Yang, J. A Binary packing material-based procedure for evaluating soil liquefaction triggering during earthquakes. *J. Geotech. Geoenviron. Eng.* **2020**, *146*, 04020040. [CrossRef]
29. Chaney, R.; Demars, K.; Brignoli, E.; Gotti, M.; Stokoe, K. Measurement of Shear Waves in Laboratory Specimens by Means of Piezoelectric Transducers. *Geotech. Test. J.* **1996**, *19*, 384–397. [CrossRef]
30. Lee, J.-S.; Santamarina, J.C. Bender Elements: Performance and Signal Interpretation. *J. Geotech. Geoenviron. Eng.* **2005**, *131*, 1063–1070. [CrossRef]
31. Zhou, Y.-G.; Chen, Y.-M. Laboratory Investigation on Assessing Liquefaction Resistance of Sandy Soils by Shear Wave Velocity. *J. Geotech. Geoenviron. Eng.* **2007**, *133*, 959–972. [CrossRef]

32. Jamiolkowski, M.; Lancellotta, R.; Lopresti, D.C.F. Remarks on the stiffness at small strains of six Italian clays. In Proceedings of the Pre-Failure Deformation of Geomaterials, Sapporo, Japan, 12–14 September 1994; pp. 817–836.
33. Liang, K.; Chen, G.; Du, X.; Xu, C.; Yang, J. A Unified Formula for Small-Strain Shear Modulus of Sandy Soils Based on Extreme Void Ratios. *J. Geotech. Geoenviron. Eng.* **2023**, *149*, 04022127. [CrossRef]
34. Zhang, Y.; Zhao, K.; Peng, Y.; Chen, G. Dynamic shear modulus and damping ratio characteristics of undisturbed marine soils in the Bohai Sea, China. *Earthq. Eng. Vib.* **2022**, *21*, 297–312.